Confined Nanocatalysts

DOI: 10.1002/anie.201204719

A Template Carbonization Strategy to Synthesize Ordered Mesoporous Silica Microspheres with Trapped Sulfonated Carbon Nanoparticles for Efficient Catalysis**

Qin Yue, Minghong Wang, Jing Wei, Yonghui Deng, Tianyi Liu, Renchao Che, Bo Tu, and Dongyuan Zhao**

Ordered mesoporous materials have attracted much attention since their discovery owing to their outstanding properties, such as tunable pore sizes and mesostructures, variable morphologies, high surface areas, and large pore volumes.[1–8] These features make them promising candidates for applications including catalysis,[9] adsorption and separation,[10] chemical sensing,[11] and biomedicine.[12] To date, significant advances have been achieved in the synthesis of mesoporous materials, particularly in the soft templating approach using surfactants or block copolymers as the templates (structure-directing agents), and enormous ordered mesoporous materials with variable pore structures, pore sizes, and framework compositions have been prepared.

Apart from exploring the methods of synthesis and strategies, considerable efforts have been devoted to designing functional ordered mesoporous materials by introducing functional nanomaterials or organic groups for practical applications. For example, using sol–gel chemistry, many functional mesoporous composites have been synthesized by coating functional nanoparticles.[13,14] Furthermore, functional organic groups or nanoparticles have been introduced into mesopores, resulting in various functional mesoporous materials that are useful in drug delivery, chemical sensing, and catalysis.[15–19] Particularly the immobilization of sulfonic acid groups (-SO_3H) in mesopores have aroused great research interest because the mesoporous materials can provide a large accessible surface area for supporting high density of acidic sites, thus serving as efficient solid Brønsted acids.[18] Compared to traditional homogeneous acid catalysts (such as H_2SO_4, $AlCl_3$, BF_3), the novel heterogeneous catalysts are environmentally benign and can be readily recycled from reaction medium, thus reducing the energy consumption for the production of chemicals.

To introduce sulfonic acid groups on the pore walls of mesoporous silica materials, typical methods involve the attachment of sulfur-containing organic silanes (for example −SH, −S−S−) by post-grafting or co-condensation and subsequent oxidation with hydrogen peroxide.[20] Van Rhijn et al.[18a] first reported the synthesis of ordered mesoporous silicas functionalized with SO_3H groups using co-condensation or post-modification. The obtained SO_3H-functionalized mesoporous silicas exhibited good performance in catalyzing the condensation of 2-methylfuran with acetone with high conversion (85%) and selectivity (96%) toward the target product 2,2-bis(5-methylfuryl)propane. By contrast, traditional microporous solid acids, such as H-β and H-US-Y zeolites, exhibited much lower conversion (ca. 60%) and selectivity (ca. 70%) owing to the undesired fast formation and adsorption of tarry oligomeric compounds in the narrow zeolite pores and subsequent catalyst deactivation. This result suggests that the immobilization of SO_3H groups in mesoporous silicas with larger pore is more favorable for catalysis. Although mesoporous silicas functionalized with the SO_3H groups can be easily synthesized by the post-grafting or co-condensation, these methods allow for only a limited amount of functional silanes to be used so as to avoid the damage of ordered mesostructure or pore blocking, resulting in a low density of sulfonic acid groups anchored in the pore walls. Recently, Nakajima et al.[21] synthesized sulfonated carbon-containing mesoporous silica SBA-15 fibers by carbonization of the impregnated glucose in the pores of SBA-15, followed with a sulfonation treatment. The mesoporous carbon/silica functionalized with SO_3H groups exhibited a good catalytic performance in the dimerization of α-methylstyrene; however, through this post impregnation, it is difficult to control the sulfonated carbon distribution and avoid pore blocking. Therefore, development of novel approaches and strategies to the synthesis of functionalized mesoporous heterogeneous solid acidic catalysts is of great importance and interest.

Herein, we demonstrate a facile template carbonization strategy to synthesize ordered large-pore mesoporous silica microspheres with sulfonated carbon nanoparticles trapped inside the accessible mesopores through a solvent-evaporation-induced aggregating assembly (EIAA) approach. In this approach, amphiphilic poly(ethylene oxide)-*b*-polystyrene (PEO-*b*-PS) and tetraethylorthorsilicate (TEOS) were used

[*] Q. Yue, M. H. Wang, J. Wei, Prof. Dr. Y. H. Deng, T. Y. Liu, Prof. Dr. R. C. Che, Prof. Dr. B. Tu, Prof. Dr. D. Y. Zhao
Department of Chemistry, Advanced Materials Laboratory
Key Laboratory of Smart Drug Delivery, Ministry of Education
Fudan University, Shanghai 200433 (China)
E-mail: yhdeng@fudan.edu.cn
dyzhao@fudan.edu.cn
Homepage: http://www.mesogroup.fudan.edu.cn/

[**] This work was supported by the NSF of China (20890123, 51172047, and 21073040), the National Key Basic Research Program (2010CB933901, 2009CB930400, and 2012CB224805), the Innovation Program of Shanghai Municipal Education Commission (13ZZ004), Shanghai Rising Star Project of STCSM (12QH1400300) and School of Pharmacy, Fudan University and The Open Project Program of Key Lab of Smart Drug Delivery (Fudan University), Ministry of Education, China.

Supporting information for this article is available on the WWW under http://dx.doi.org/10.1002/anie.201204719.

as a template and silica source, respectively. Through consecutive treatments of the PEO-*b*-PS/silica composite microspheres, including hydrothermal aging, in situ carbonization, and sulfonation, highly ordered mesoporous silica microspheres with sulfonated carbon nanoparticles confined in the mesopores (OMS/C-SO_3H) were obtained. In this synthesis, PEO-*b*-PS molecules not only were employed as a template for creation of uniform mesopores, but could also be fully utilized as a carbon source for in situ generation of carbon nanoparticles in the mesopores, thus avoiding the waste of organic templates and making it unnecessary to introduce foreign carbon sources by tedious impregnation. The OMS/C-SO_3H microspheres possess an ordered mesoporous structure with symmetry of $Fm\bar{3}m$, large accessible mesopores (15.4 nm), high surface area (612 $m^2 g^{-1}$), large pore volume (0.48 $cm^3 g^{-1}$), and sulfonated carbon nanoparticles (6.0 nm) trapped in the mesopores. As a result of the unique mesostructure and the abundant SO_3H groups, the OMS/C-SO_3H microspheres show an excellent catalytic performance in the condensation reaction of benzaldehyde with ethylene alcohol with a high conversion (93 %) and good reusability.

The amphiphilic PEO-*b*-PS block copolymers can be dissolved well in an acidic THF/H_2O solution (5:3 v/v) containing a certain amount of the silica source (TEOS). After evaporation of the THF solvent, a milky colloidal solution of silica/PEO-*b*-PS composites was formed as a result of the co-assembly of template molecules and silicate oligomers and the aggregation of PEO-*b*-PS/silica composite micelles.[6a,8] Scanning electron microscopy (SEM) shows that the as-made silica/PEO-*b*-PS composites collected by centrifugation have a regular spherical shape with the size ranging from 1.5 to 8.0 μm (Figure 1 a). After a hydrothermal treatment at 100 °C and further in-situ carbonization of the PEO-*b*-PS templates at 600 °C in N_2, the obtained carbon-containing ordered mesoporous silica (OMS/C-HT100-600N) materials show a retained spherical morphology (Figure 1 b), which is indicative of a good thermal stability of the composites. Ordered arrays of mesopores can be clearly visible in the surface of the microspheres, confirming an ordered mesostructure (Figure 1 b, inset). The OMS/C-HT100-600N sample is gray in color, implying that some of carbon residuals are remained in the mesopores of the obtained mesoporous silica through an in situ carbonization (Supporting Information, Figure S1). In contrast, the mesoporous silica materials (OMS/C-HT100-600A) obtained by calcination of the composites at 600 °C in air is white in color, suggesting a complete removal of the PEO-*b*-PS template by the combustion.

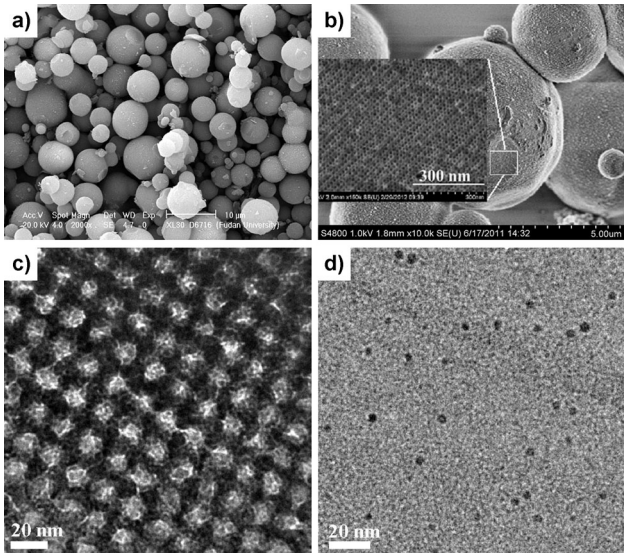

Figure 1. SEM images of a) the as-made PEO-*b*-PS/silica composite and b) OMS/C-HT100-600N, and TEM images of c) OMS/C-HT100-600N viewed from the [110] direction and d) the carbon nanoparticles obtained by etching out silica species in the OMS/C-HT100-600N sample. The inset in (b) is the magnified FESEM image of OMS/C-HT100-600N.

Small-angle X-ray scattering (SAXS) patterns of the silica/PEO-*b*-PS-HT100 sample obtained after the hydrothermal treatment of the as-made composite at 100 °C for 12 h show three scattering peaks with q values of 0.369, 0.711, and 0.953 nm^{-1}, which can be exactly indexed to the 111, 311, and 420 reflections of highly ordered face centered cubic (*fcc*) mesostructure with a space group of $Fm\bar{3}m$ (Supporting Information, Figure S2a). After further carbonization at 600 °C in N_2, the resulting OMS/C-HT100-600N sample shows similar SAXS patterns with four well-resolved scattering peaks assigned to face-centered cubic (*fcc*) $Fm\bar{3}m$ symmetry (Supporting Information, Figure S2b). Owing to the enhanced mass contrast caused by the carbonization of PEO-*b*-PS template molecules, the intensity of the scattering peaks was increased significantly; while the shift of scattering peaks toward lower q values is ascribed to the shrinkage of the silica framework caused by the further condensation after carbonization treatment. The unit cell parameter a of the sample OMS/C-HT100-600N calculated from the SAXS data is about 27.2 nm, which is slightly less than that (29.4 nm) of OMS/C-HT100 (Table 1). After sulfonation, the obtained OMS/C-SO_3H sample shows SAXS patterns similar to those of OMS/C-HT100-600N, suggesting that the sulfonation treatment has little influence on the ordered mesostructure (Supporting Information, Figure S2c). It is worth noting that the hydrothermal treatment of the as-made silica/PEO-*b*-PS composite at higher temperature (such as 130 °C) can destroy the ordered mesostructure, as revealed by the SAXS and TEM measurements (Supporting Information, Figure S3).

Table 1: Texture properties of the ordered mesoporous silica with carbon nanoparticles templated from PEO-*b*-PS copolymers.

Sample	D [nm][a]	a_0 [nm][b]	W [nm][c]	S_{bet} [$m^2 g^{-1}$][d]	S_m [$m^2 g^{-1}$][e]	V [$cm^3 g^{-1}$][f]
PEO-*b*-PS/ silica- HT100	–	29.4	–	–	–	–
OMS/C-HT100-600N	15.8	27.2	<5.0	620	186	0.50
OMS/C-HT100-600A	15.9	27.0	<5.0	628	203	0.51
OMS/C-SO_3H	15.4	27.0	<5.0	612	162	0.48

[a] Pore size calculated from the BdB model. [b] Unit cell parameter calculated from SAXS results. [c] Primary pore window size. [d] BET surface area. [e] Micropore surface areas. [f] Total pore volume.

Transmission electron microscopy (TEM) images show that the OMS/C-HT100-600N sample has a high degree of periodicity over large domain as viewed from the [100], [110], and [111] directions, (Supporting Information, Figure S4). It further confirms that the mesostructure templated from PEO-*b*-PS have a highly ordered cubic symmetry ($Fm\bar{3}m$) by the versatile EIAA approach. The uniform and spherical pores are clearly visible in the images, implying that the ordered mesoporous silicas are constructed through the close packing of uniform spherical micelles. Moreover, tiny carbon nanoparticles can be clearly observed in the spherical mesopores (Figure 1c), which suggests that the PEO-*b*-PS templates are carbonized in situ in the mesopores. To further confirm this result, the OMS/C-HT100-600N sample was treated with an HF solution (10 wt%) to dissolve the silica framework, and black carbon residuals were collected by high-speed centrifugation and washing with ethanol. The TEM characterization clearly shows that carbon nanoparticles are relatively uniform with the size of about 6.0 nm (Figure 1d). These results provide new evidence that the PEO-*b*-PS micelles underwent an in situ carbonization in the confined space of the uniform mesopores, and as a result, the carbon nanoparticles are highly dispersed throughout the mesoporous silica spheres (Supporting Information, Figure S4d, inset). After the sulfonation treatment, TEM images of the obtained OMS/C-SO_3H show that the ordered mesostructure is well-retained (Supporting Information, Figure S5), which is consistent with the SAXS results (Supporting Information, Figure S2c) and further confirms the excellent stability of the ordered mesostructure even under the harsh conditions. The sulfonated carbon nanoparticles can be seen in the magnified TEM images (Supporting Information, Figure S5c,d). It implies that the carbon nanoparticles are well-preserved in the mesopores of OMS/C-SO_3H microspheres after the sulfonation treatment.

N_2 adsorption–desorption isotherms of the OMS/C-HT100-600N sample show type IV curves with a sharp capillary condensation step in the relative pressure range of 0.76–0.86 (Figure 2a, ■), indicative of a large and uniform mesopore size. The isotherms display a large H_2-type hysteresis loop with delayed capillary evaporation located at a relative pressure of about 0.45, suggesting that the sample OMS/C-HT100-600N possesses large caged mesopores with a small window size of less than 5.0 nm.[22] The pore size distribution curve derived from the adsorption branch using BdB model[23] shows a bimodal porous structure with a uniform primary mesopore centered at 15.8 nm (Figure 2b, ●). The secondary mesopore with a wide pore size distribution (3–7 nm) is ascribed to the irregular holes in the primary pore wall formed by the tunneling effect from the hydrothermal treatment. Therefore, the primary spherical mesopores are well-connected and highly accessible. The BET surface area, micropore surface, and pore volume were calculated to be 620, 186 $m^2 g^{-1}$, and 0.50 $cm^3 g^{-1}$, respectively (Table 1). Compared to OMS/C-HT100-600N, the OMS/C-HT100-600A sample has similar N_2 adsorption–desorption isotherms (Supporting Information, Figure S6) and texture properties (Table 1). It suggests that the carbon nanoparticles have little effect on the pore structure and pore connection of the ordered mesoporous silicas. After the sulfonation, the obtained OMS/C-SO_3H sample shows N_2 adsorption-desorption isotherms (Figure 2a, ○) similar to those of the sample OMS/C-HT100-600N, further confirming that the sulfonation treatment has no substantial effect on the ordered mesoporous siliceous framework. The pore size distribution has a similar bimodal porous structure, with primary and secondary mesopores centered at 15.4 and 5.0 nm (Figure 2b, □), respectively, both slightly less than those of OMS/C-HT100-600N, which is probably due to the introduction of polar hydrophilic groups in the carbon nanoparticles.[20] The BET surface area, micropore surface, and pore volume of the sample OMC-SO_3H are calculated to be 612, 162 $m^2 g^{-1}$, and 0.48 $cm^3 g^{-1}$, respectively (Table 1).

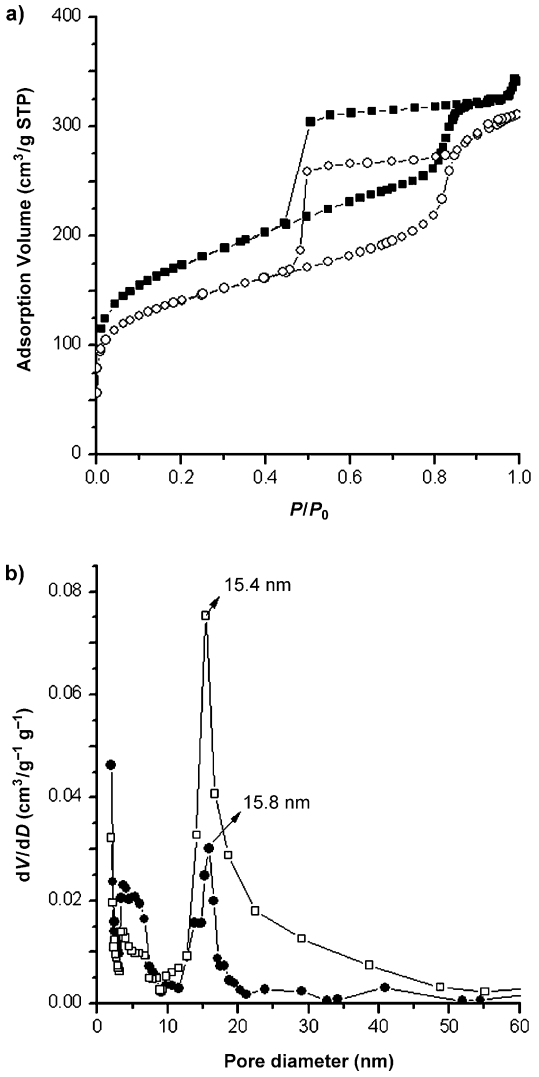

Figure 2. a) N_2 adsorption–desorption isotherms and b) pore size distribution of OMS/C-HT100-600N (■, ●) and OMS/C-SO_3H samples (□, ○).

The thermogravimetric analysis curve of the sample OMS/C-SO_3H (Supporting Information, Figure S7) recorded from 25 to 800 °C in air shows two steps of weight loss. The first step occurred in the range of 25–100 °C and can be attributed to the removal of physically absorbed water, accounting for

weight loss of about 4.3 wt%, while the second weight loss (ca. 3.5 wt%) in the range of 200–800°C is due to the continuous combustion of carbonaceous species in the mesopores. No appreciable weight loss is observed in the range of 100–200°C, suggesting that the sample is relatively stable in this temperature range. FTIR spectroscopy analysis shows that, before the sulfonation treatment, the OMS/C-HT100-600N sample (Supporting Information, Figure S8a) shows typical absorption peaks at 1090, 2930, and 2845 cm^{-1}, attributed to Si–O–Si, CH_2, and CH_3 vibrations, respectively. The absorption at 1641 cm^{-1} is from the adsorbed water. These results indicate that minor organic moieties remain in the carbon nanoparticles in the mesopores of OMS/C-HT100-600N because of the incomplete carbonization of PEO-*b*-PS template molecules. After sulfonation, only a new band at 1402 cm^{-1} is observed in the OMS/C-SO_3H sample (Supporting Information, Figure S8b) because many peaks overlap with those of the silica framework. To eliminate this interference, the silica was removed from OMS/C-SO_3H using hydrofluoric acid (10%). The FTIR spectrum of the obtained carbon residual sample (Supporting Information, Figure S8c) clearly shows peaks at 1190 and 1036 cm^{-1} assigned to the SO_3H groups,[24] confirming a successful introduction of sulfonic acid groups, while the peaks at 1632 and 1402 cm^{-1} are from C=O and O–H, respectively, indicating the presence of minor amount of carboxyl groups. Element analysis shows that the sulfur content is about 1.0 wt%, which corresponds to a sulfuric acid group concentration of 0.031 mmol g^{-1} assuming that the sulfur only takes the form of SO_3H in the sulfonated sample. This value is slightly lower than that (0.034 mmol g^{-1}) obtained from our acid–base titration measurements,[25] which is probably due to the presence of small amount of carboxyl groups, and is also much lower than those reported previously.[18,21,24]

As the size of the carbon nanoparticles is smaller than the mesopore size (15.4 nm) but larger than the window size (< 5.0 nm), the sulfonated carbon nanoparticles can be effectively and stably confined in the mesopores. The unique mesostructured OMS/C-SO_3H microspheres can serve as a novel nanoreactor. In this study, the catalysis performance of this novel functional mesoporous microsphere was investigated by using it as a heterogeneous solid catalyst for the condensation of benzaldehyde (PhCHO) with ethylene glycol in cyclohexane. For comparison, microporous zeolite HZSM-5 (Si/Al = 35), mesoporous silica MCM41-SO_3H, and OMS/C-HT100-600 A-SO_3H were also prepared and used as the heterogeneous acid catalysts (see the Supporting Information for experimental details). From Figure 3a, it can be seen that the conversion of benzaldehyde can ramp up to 66% after reaction for 0.5 h and quickly reach 89% after running for 1 h, indicating an excellent catalytic performance owing to the high concentration of sulfonic acid groups. Prolonging the reaction time to 2 h only slightly increases the conversion to about 93%, suggesting that the reaction can quickly reach a thermodynamic equilibrium with a high conversion. In contrast, despite their higher concentration of acidic sites, HZSM-5-35, MCM41-SO_3H, and OMS/C-HT100-600A-SO_3H exhibit a much lower conversion of benzaldehyde (58.0, 62.4, and 63.5%, respectively) after

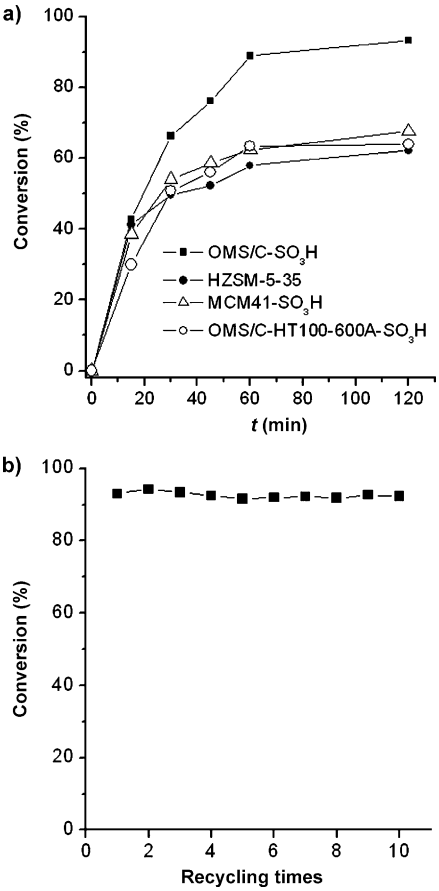

Figure 3. a) The conversion of benzaldehyde as a function of reaction time during the condensation reaction of benzaldehyde with ethylene glycol using OMS/C-SO_3H (■), HZSM-5-35 (●), MCM41-SO_3H (△), and OMS/C-HT-600 A-SO_3H (○) as catalysts. b) Catalytic activity of the reused OMS/C-SO_3H microspheres for the condensation of benzaldehyde with ethylene glycol.

reaction for 1 h. This is mainly due to their much narrow pore channels or reduced pore entrances that hamper the contact of reactants and transportation of both reactants and desorption of products. To study its reusability, the OMS/C-SO_3H catalyst were recycled by centrifugation, thoroughly washed with ethanol, and dried in vacuum. As shown in Figure 3b, the conversion of benzaldehyde can be maintained above 90% even after running 10 times, indicating an excellent reusability. The outstanding catalytic performance of the heterogeneous solid acid catalyst is believed to be attributed to its unique designed porous structure that has well-connected and easily accessible large mesopores, highly sulfonated carbon nanoparticles in the pores, and a stable silica framework.

In conclusion, a facile template carbonization strategy has been demonstrated for the synthesis of novel ordered mesoporous silica microspheres (OMS/C-SO_3H) with sulfonated carbon nanoparticles stably trapped in the highly accessible large mesopores. The synthesis is accomplished by a solvent-evaporation-induced aggregating assembly of PEO-*b*-PS template molecules and TEOS in an acidic THF/water solution, followed with an in situ carbonization of template molecules and sulfonation treatment of the residual carbon

nanoparticles. The obtained OMS/C-SO_3H microspheres have an ordered mesostructure with *fcc* symmetry, large and open mesopores (ca. 15.4 nm), high surface area (ca. 612 $m^2 g^{-1}$), large pore volume (0.48 $cm^3 g^{-1}$), and uniform sulfonated carbon nanoparticles (ca. 6.0 nm) stably confined in the mesopores. As a result of the unique open mesoporous silica structure and highly dispersed SO_3H-bearing carbon nanoparticles, the OMS/C-SO_3H microspheres show excellent catalytic performance in the condensation reaction of benzaldehyde with ethylene alcohol with a high conversion (93%) and good reusability. It is believed that the carbon nanoparticles can be modified with other functional groups, such as NH_2, organic chromophore groups, and drug molecules, which can lead to various functional mesoporous materials for applications in separation, drug delivery, and sensing. Furthermore, this design concept could be used to synthesize various functional porous materials with diverse framework compositions and trapped functional nanoparticles of carbon or metal (or metal oxides).

Received: June 16, 2012
Revised: July 25, 2012
Published online: September 11, 2012

Keywords: block copolymers · carbon nanoparticles · heterogeneous catalysis · mesoporous materials · sulfonation

[1] a) C. T. Kresge, M. E. Leonowicz, W. J. Roth, J. C. Vartuli, J. S. Beck, *Nature* **1992**, *359*, 710; b) D. Y. Zhao, J. L. Feng, Q. S. Huo, N. Melosh, G. H. Fredrickson, B. F. Chmelka, G. D. Stucky, *Science* **1998**, *279*, 548.

[2] Y. Fang, D. Gu, Y. Zou, Z. X. Wu, F. Y. Li, R. C. Che, Y. H. Deng, B. Tu, D. Y. Zhao, *Angew. Chem.* **2010**, *122*, 8159; *Angew. Chem. Int. Ed.* **2010**, *49*, 7987.

[3] Y. H. Deng, J. Liu, C. Liu, D. Gu, Z. K. Sun, J. Wei, J. Y. Zhang, L. J. Zhang, B. Tu, D. Y. Zhao, *Chem. Mater.* **2008**, *20*, 7281.

[4] F. Q. Zhang, D. Gu, T. Yu, F. Zhang, S. H. Xie, L. J. Zhang, Y. H. Deng, Y. Wan, B. Tu, D. Y. Zhao, *J. Am. Chem. Soc.* **2007**, *129*, 7746.

[5] S. Che, Z. Liu, T. Ohsuna, K. Sakamoto, O. Terasaki, T. Tatsumi, *Nature* **2004**, *429*, 281.

[6] a) Y. H. Deng, T. Yu, Y. Wan, Y. F. Shi, Y. Meng, D. Gu, L. J. Zhang, Y. Huang, C. Liu, X. J. Wu, D. Y. Zhao, *J. Am. Chem. Soc.* **2007**, *129*, 1690; b) Y. H. Deng, Y. Cai, Z. K. Sun, D. Gu, J. Wei, W. Li, X. H. Guo, J. P. Yang, D. Y. Zhao, *Adv. Funct. Mater.* **2010**, *20*, 3658.

[7] Y. H. Deng, C. Liu, D. Gu, T. Yu, B. Tu, D. Y. Zhao, *J. Mater. Chem.* **2008**, *18*, 91.

[8] a) J. Wei, H. Wang, Y. H. Deng, Z. K. Sun, L. Shi, B. Tu, M. Luqman, D. Y. Zhao, *J. Am. Chem. Soc.* **2011**, *133*, 20369; b) J. Wei, Q. Yue, Z. K. Sun, Y. H. Deng, D. Y. Zhao, *Angew. Chem.* **2012**, *124*, 6253; *Angew. Chem. Int. Ed.* **2012**, *51*, 6149.

[9] a) A. Corma, *Chem. Rev.* **1997**, *97*, 2373; b) S. H. Joo, S. J. Choi, I. Oh, J. Kwak, Z. Liu, O. Terasaki, O. R. Ryoo, *Nature* **2001**, *412*, 169; c) A. Taguchi, F. Schuth, *Microporous Mesoporous Mater.* **2004**, *77*, 145.

[10] a) A. Vinu, V. Murugesan, O. Tangermann, M. Hartmann, *Chem. Mater.* **2004**, *16*, 3056; b) A. M. Liu, K. Hidajat, S. Kawi, D. Y. Zhao, *Chem. Commun.* **2000**, 1145; c) B. L. Newalkar, N. V. Choudary, P. Kumar, S. Komarneni, T. S. G. Bhat, *Chem. Mater.* **2002**, *14*, 304; d) Z. K. Sun, Y. H. Deng, J. Wei, D. Gu, B. Tu, D. Y. Zhao, *Chem. Mater.* **2011**, *23*, 2176.

[11] a) T. Yamada, H. S. Zhou, H. Uchida, M. Tomita, Y. Ueno, T. Ichino, I. Honma, K. Asai, T. Katsube, *Adv. Mater.* **2002**, *14*, 812; b) T. Waitz, T. Wagner, T. Sauerwald, C. D. Kohl, M. Tiemann, *Adv. Funct. Mater.* **2009**, *19*, 653.

[12] a) J. L. Liu, C. Y. Li, F. Y. Li, *J. Mater. Chem.* **2011**, *21*, 7175; b) I. I. Slowing, B. G. Trewyn, S. Giri, V. S. Y. Lin, *Adv. Funct. Mater.* **2007**, *17*, 1225; c) M. A. Vallet-Regí, L. Ruiz-González, I. Izquierdo-Barba, J. M. González-Calbet, *J. Mater. Chem.* **2006**, *16*, 26.

[13] a) S. H. Joo, J. Y. Park, C. K. Tsung, Y. Yamada, P. Yang, G. A. Somorjai, *Nat. Mater.* **2009**, *8*, 126; b) I. Lee, Q. Zhang, J. P. Ge, Y. D. Yin, F. Zaera, *Nano Res.* **2011**, *4*, 115; c) I. Pastoriza-Santos, J. Pérez-Juste, L. M. Liz-Marzán, *Chem. Mater.* **2006**, *18*, 2465.

[14] a) Y. H. Deng, Y. Cai, Z. K. Sun, D. Y. Zhao, *Chem. Phys. Lett.* **2011**, *510*, 1; b) L. Zhang, S. Z. Qiao, Y. G. Jin, Z. G. Chen, H. C. Gu, G. Q. Lu, *Adv. Mater.* **2008**, *20*, 805; c) Y. H. Deng, D. W. Qi, C. H. Deng, X. M. Zhang, D. Y. Zhao, *J. Am. Chem. Soc.* **2008**, *130*, 28; d) Y. H. Deng, Y. Cai, Z. K. Sun, J. Liu, C. Liu, J. Wei, W. Li, C. Liu, Y. Wang, D. Y. Zhao, *J. Am. Chem. Soc.* **2010**, *132*, 8466.

[15] a) R. M. Rioux, H. Song, D. Hoefelmeyer, J. D. Hoefelmeyer, P. Yang, G. A. Somorjai, *J. Phys. Chem. B* **2005**, *109*, 2192; b) L. Mercier, T. J. Pinnavaia, *Environ. Sci. Technol.* **1998**, *32*, 2749; c) M. Vallet-Regí, F. Balas, D. Arcos, *Angew. Chem.* **2007**, *119*, 7692; *Angew. Chem. Int. Ed.* **2007**, *46*, 7548.

[16] a) R. Liu, Y. Zhang, X. Zhao, A. Agarwal, L. J. Mueller, P. Y. Feng, *J. Am. Chem. Soc.* **2010**, *132*, 1500; b) R. Métivier, I. Leray, B. Lebeau, B. Valeur, *J. Mater. Chem.* **2005**, *15*, 2965.

[17] a) G. Wirnsberger, B. J. Scott, G. D. Stucky, *Chem. Commun.* **2001**, 119; b) K. Sarkar, K. Dhara, M. Nandi, P. Roy, A. Bhaumik, P. Banerjee, *Adv. Funct. Mater.* **2009**, *19*, 223.

[18] a) W. M. Van Rhijn, D. E. De Vos, B. F. Sels, W. D. Bossaert, P. A. Jacobs, *Chem. Commun.* **1998**, 317; b) M. H. Lim, C. F. Blanford, A. Stein, *Chem. Mater.* **1998**, *10*, 467; c) W. D. Bossaert, D. E. De Vos, W. M. Van Rhijn, J. Bullen, P. J. Grobet, P. A. Jacobs, *J. Catal.* **1999**, *182*, 156; d) D. Margolese, J. A. Melero, S. C. Christiansen, B. F. Chmelka, G. D. Stucky, *Chem. Mater.* **2000**, *12*, 2448.

[19] a) C. M. Yang, B. Zibrowius, F. Schuth, *Chem. Commun.* **2003**, 1772; b) H. H. G. Tsai, G. L. Jheng, H. M. Kao, *J. Am. Chem. Soc.* **2008**, *130*, 11566; c) R. J. P. Corriu, L. Datas, Y. Guari, A. Mehdi, C. Reye, C. Thieuleux, *Chem. Commun.* **2001**, 763.

[20] X. Q. Wang, R. Liu, M. M. Waje, Z. W. Chen, Y. S. Yan, K. N. Bozhilov, P. Y. Feng, *Chem. Mater.* **2007**, *19*, 2395.

[21] K. Nakajima, M. Okamura, J. N. Kondo, K. Domen, T. Tatsumi, S. Hayashi, M. Hara, *Chem. Mater.* **2009**, *21*, 186.

[22] a) M. Kruk, M. Jaroniec, *Chem. Mater.* **2003**, *15*, 2942; b) P. I. Ravikovitch, A. V. Neimark, *Langmuir* **2002**, *18*, 9830; c) M. Kruk, J. R. Matos, M. Jaroniec, *Colloids Surf. A* **2004**, *241*, 27.

[23] J. C. P. Broekhoff, J. H. deBoer, *J. Catal.* **1967**, *9*, 8.

[24] a) A. Stein, Z. Y. Wang, M. A. Fierke, *Adv. Mater.* **2009**, *21*, 265; b) R. Xing, N. Liu, Y. M. Liu, H. H. Wu, Y. W. Jiang, L. Chen, M. Y. He, P. Wu, *Adv. Funct. Mater.* **2007**, *17*, 2455; c) C. D. Liang, Z. J. Li, S. Dai, *Angew. Chem.* **2008**, *120*, 3754; *Angew. Chem. Int. Ed.* **2008**, *47*, 3696; d) R. Xing, Y. M. Liu, Y. Wang, L. Chen, H. H. Wu, Y. W. Jiang, M. Y. He, P. Wu, *Microporous Mesoporous Mater.* **2007**, *105*, 41.

[25] C. W. Jones, K. Tsuji, M. E. Davis, *Nature* **1998**, *393*, 52.

